

STUDY OF MECHANICAL PROPERTIES AND FAILURE MECHANISM OF CFRP-ALUMINUM ALLOY SELF-PIERCING RIVETED-ADHESIVE JOINTS

Y. Q. Yan, S. Xu,* Y. F. Xing, H. L. Bian, and H. F. Wu

Keywords: carbon fiber-reinforced polymers, riveted-bonded joining, failure mechanism

The mechanical properties and failure mechanisms of self-piercing riveted-adhesive joints of carbon fiber-reinforced polymers/6061-T6 aluminum plates was investigated. The effects of riveting pressure, aluminum surface treatment, and lap length on the mechanical properties of the joints were analyzed. The microscopic morphology of the joint at each stage of the failure process was obtained by tensile-shear test and electron microscopy scan, on which the changes of CFRP, aluminum plate, rivet, and adhesive layer at different stages were further discussed to reveal the failure mechanism of the joint. The results showed that the joint strength could be improved by appropriately increasing the riveting pressure. The surface treatment of aluminum plate could improve the surface properties of the joint, and the joint strength showed a trend of first increasing and then decreasing with the increase of the sandpaper mesh. Increasing the lap length led to an increase in joint strength; however, when the lap length was increased to a certain value, the increase in joint strength was not obvious. The failure process of the adhesive riveted specimen was from the failure of the adhesive layer to the failure of the rivet, and after rivet failure, the joint failed completely.

1. Introduction

In recent years, the popularity of new energy vehicles has put forward higher requirements for vehicle lightweighting [1-2]. Automotive manufacturers prefer to adopt multi-material hybrid body structures [3]. Aluminum alloy is the preferred material for automotive lightweighting due to its low density, high specific strength and stiffness, while carbon fiber-reinforced plastic (CFRP), which is widely used in the field of aviation and marine, has been popularly used in au-

Shanghai University of Engineering Science, 333 Longteng Road, Songjiang District, Shanghai 201620, China

*Corresponding author; e-mail: xytongxing376@sina.com

Original article submitted October 17, 2022; revision submitted May 5, 2023.

tomotive bodywork for its excellent mechanical properties, high specific strength and stiffness, designability, fatigue and corrosion resistances. Therefore, the realization of an effective and reliable connection between CFRP and aluminum alloy has become one of the important directions in the development of automotive lightweighting.

The common techniques for joining plates currently include bolting, riveting, bonding, and welding. It is well known that these techniques are becoming mature for joining metal sheets. However, in the joining of composites to metals, these joining methods encounter some problems, especially in the joining of CFRPs. For instance, bolting and riveting need to open holes in the CFRP laminate, which can cause fracture failure of carbon fibers and affect the overall performance of CFRP. In addition, there is also a large stress concentration at the bolt and rivet holes, which reduces the overall strength of the structure [4]. As for welding, although the stress concentration phenomenon is reduced to some extent, the temperature of the welding pool is high, and the connected plates are highly susceptible to reinforcing phase melting, dissolution, sublimation, and interfacial reactions, resulting in the carbon fiber damage fracture in CFRP and tissue failure [5]. And for the adhesive structure, it has uniform stress distribution, light weight, and simple operation, which allows the connection of dissimilar materials without destroying them [6]; however, the anti-peel ability of the joint is low, and the adhesive is prone to aging and brittle fracture, reducing the overall strength of the structure [7].

In response to the above-mentioned problems of a single connection method, many scholars had tried to explore the mechanism of these problems and reduce the magnitude of the joint strength reduction by establishing relevant mathematical optimization models [8] and simulation models [9, 10], improving the material properties of the connected parts themselves [11], improving the joint structure [12], selecting suitable connection process parameters [13], etc. However, it was still impossible to further improve the mechanical properties of the composite and metal joints. Therefore, researchers tried to apply two joining techniques in combination with each other for the joining of composites to metals [14-17]. Among them, the self-piercing riveting-gluing connection has become a hot research concern by combining the self-piercing riveting and gluing processes to make the composite and metal joint with both the peel resistance of riveting and the sealing performance of bonding [18].

To further improve the joint performance, a series of studies have been conducted by adjusting the plate parameters of the composite and metal and the material of the rivet. Franco et al [19] found that the CFRP lay-up method played a decisive role in the tensile strength of the adhesive layer by performing tensile shear tests on adhesive riveted joints made of aluminum plate and composite materials. Marannano et al [20] performed tensile experiments and finite element analysis studies on the mechanical properties of adhesive riveted double-lap joints between aluminum and CFRP laminates. Results showed that using steel rivets could get better mechanical properties for hybrid Al-CFRP joints than other materials of rivets. Liu et al [21] found that an appropriate increase in the thickness of the CFRP plate was beneficial to improving the strength and energy absorption of the CFRP-aluminum alloy joint. In addition, researchers have analyzed the effect of different structural parameters on the mechanical properties of joints, including the number and distribution of rivets and the lap length, etc. Franco et al [22, 23] gradually obtained the optimum rivet spacing for the optimum tensile strength of CFRP-aluminum alloy joints by means of static tensile and fatigue tests. Fiore et al [24] found that the curing time of the resin in the adhesive and the rivet insertion time had a significant effect on the performance of adhesive-riveted joints made of aluminum and glass fiber-reinforced composites by tensile experiments. Roškowicz et al [25] carried out the fatigue experiments and numerical analysis for CFRP-aluminum alloy adhesive-riveted hybrid joints and found that placing the rivets one rivet hole diameter away from the edge increased the strength of the hybrid joints. Cui et al [26] found that applying a square array layout to rivets can improve the shear strength of CFRP-aluminum alloy adhesive-riveted joints through shear experiments.

In general, the current research mainly focused on the evaluation of joint quality, selection of process parameters, and mechanical properties testing for the riveted-bonded joining between composites and metals. However, there are still many factors affecting the adhesive-riveted joints between composites and metals. In order to improve the quality and mechanical properties of the joints, an in-depth study on the adhesive-riveted joints between composites and metals is needed, especially on the connection mechanism and mechanical properties of the self-piercing riveted-adhesive joints between CFRP and aluminum alloys. In this paper, CFRP and 6061-T6 aluminum plates were used to prepare specimens to study

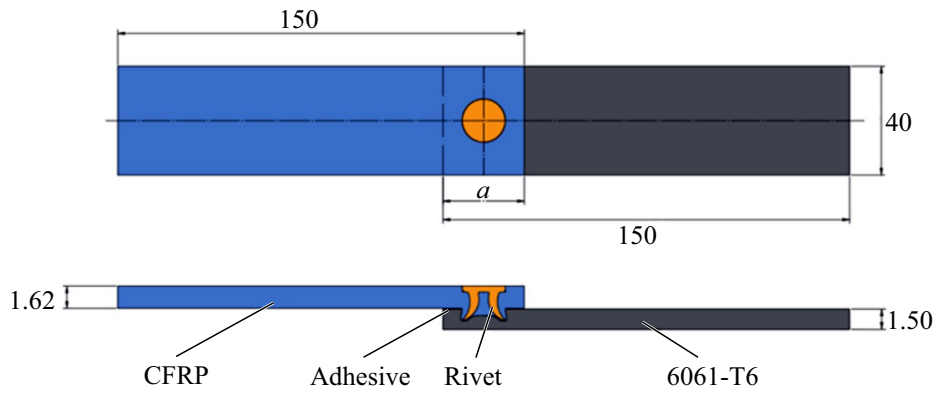


Fig. 1. Diagram of adhesive/riveted joint (mm).

TABLE 1. Properties of Materials

| Property | CFRP | 6061-T6 | ET5429 | 45#Steel |
|---------------------------|-------|---------|--------|----------|
| Tensile strength, MPa | 746 | 290 | – | 600 |
| Tensile modulus, GPa | 50.5 | – | 1 | 206 |
| Compressive strength, MPa | 337.5 | – | – | – |
| Compressive modulus, GPa | 33.2 | – | – | – |
| Yield strength, MPa | – | 240 | – | 355 |
| Shear strength, MPa | – | – | 18-22 | 370 |
| Elongation, % | – | 9 | – | 16 |

an influence of riveting pressure, aluminum surface treatment, lap length, and other process parameters on the mechanical properties of self-piercing adhesive-riveted joints, and to reveal the failure mechanism of the joints by analyzing the changes of microstructure before and after forming and at different stages of tensile testing.

2. Experimental Material and Methods

2.1. Materials

Carbon fiber-reinforced composite panels (CFRP) and 6061-T6 aluminum alloy were selected as the base sheets for the test. The CFRP with $[0/90]_{3s}$ layup was made from T300 carbon fibers and epoxy resin. As shown in Fig. 1, the length-width size of the CFRP and aluminum plates were both 150×40 mm. The upper plate was CFRP with the thickness of 1.62 mm, and the lower plate was aluminum alloy with the thickness of 1.5 mm, where a is the lap length. The adhesive selected for the test was ET5429, which was made of ET5429A epoxy resin mixed with ET5429B polyamine hardener in a ratio of 2:1; it was suitable also for most metal and composite material joints. Considering the strength of the joint, the test was carried out using 45# steel semi-hollow rivets for bonded riveting. The mechanical properties of each material were shown in Table 1.

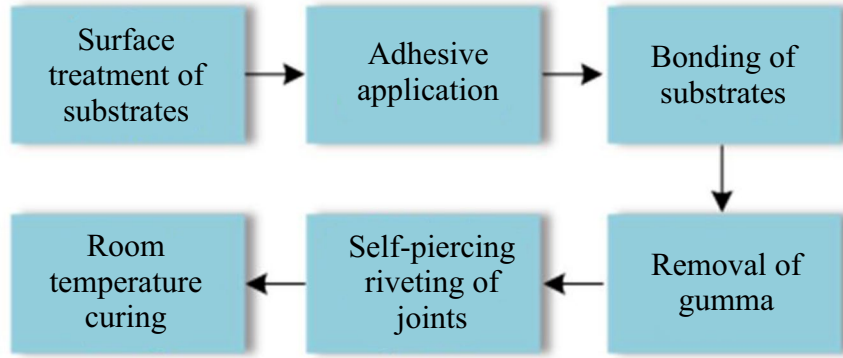


Fig. 2. Process of adhesive/rievet joint.

2.2. Joint preparation

The production process of the glued-riveted hybrid joint is shown in Fig. 2. Firstly, the CFRP plate was sanded by using sandpaper to remove the protective layer on the surface. Then, the surface debris was wiped with alcohol and the CFRP plate was dried at room temperature. In addition, using alcohol to wipe off dirt and grease from the surface of the 6061-T6 aluminum plate. Subsequently, the adhesive was squeezed onto the adhesive area on the aluminum surface using a bonding gun and the gaps between the adhesive were removed with a squeegee. The CFRP plate was placed on the aluminum plate coated with adhesive, ensuring that the overlapping areas of the upper and lower plates were bonded identically. These plates were riveted by using a hydraulic self-piercing riveting machine.

Considering the interlocking of the rivet leg and plate, the tab concave die was selected. There are two concave die parameters that affect the quality of the self-pierce riveted joint; one is the inner wall diameter d_2 , and the other is the depth h . The inner wall diameter d_2 is set to 8.8 mm according to the empirical formula [27]

$$d_2 = d_a + 0.8t_2, \quad (1)$$

where d_a is the rivet head diameter, t_2 is the lower plate thickness. The depth of the die h is related to the length of the rivet protruding from the upper and lower plates, and its size needs to be between 1.5 and 2.17 mm; so the depth of the die chosen was 2 mm.

During the self-piercing riveting process, the crimp ring was pressed against the sample and the hydraulic control device pushed the piercing downwards rapidly to form a self-piercing riveted joint between the rivet and the upper and lower plates. At the end of the riveting process, the adhesive was squeezed and spilled out of the end of the plate due to the riveting pressure in the adhesive area. The excess adhesive needed to be removed to avoid the formation of an adhesive lump after curing, which can affect the strength of the joint. Finally, the adhesive-riveted joint specimen was left to cure at room temperature for 3 days.

2.3. Experimental methods

In order to study the effect of different process parameters on the mechanical properties of CFRP-aluminum alloy adhesive-riveted joints, three parameters of riveting compression, lap length, and surface treatment of aluminum plate were selected to develop the test program, which was shown in Table 2.

MJD-200B universal testing machine was used to perform the tensile-shear test of the joint. The tensile loading rate of the equipment ranges from 0.001 to 500 mm/min, and the maximum tensile force can reach 200 kN. 40×40 mm shims were padded at both ends of the joint during the test to prevent additional bending moments during the tensile loading. To

TABLE 2. Experimental Properties

| Groups | Lap length, mm | Pressure, MPa | Type of surface treatment of aluminum plate |
|--------|----------------|---------------|---|
| 1 | 30 | 160 | Sandpaper of 400 mesh |
| | | 180 | |
| | | 200 | |
| 2 | 25 | 200 | Sandpaper of 400 mesh |
| | 30 | | |
| | 35 | | |
| | 40 | | |
| | 45 | | |
| 3 | 30 | 200 | Sandpaper of 180 mesh |
| | | | Sandpaper of 400 mesh |
| | | | Sandpaper of 600 mesh |
| | | | Sandpaper of 800 mesh |
| | | | Sandpaper of 1000 mesh |
| | | | Alcohol cleaning Ultrasonic cleaning |

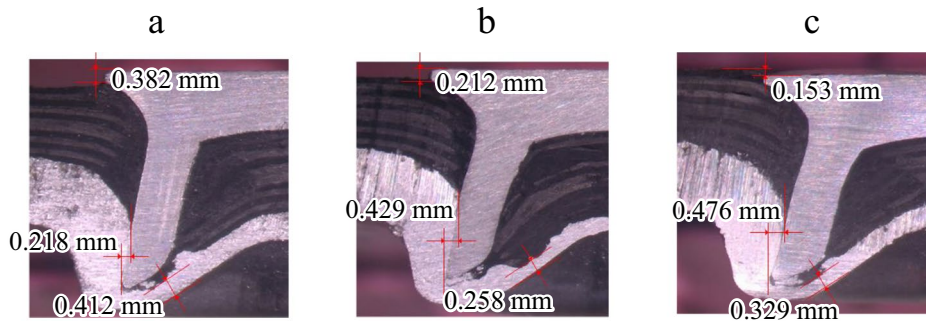


Fig. 3. Profiles of three riveting pressures.

ensure the reliability of the test results, each group of adhesive riveted joints was subjected to five repetitive pull-shear tests with the loading rate of 5 mm/min.

3. Results and Discussion

3.1. Effect of process parameters

3.1.1. Riveting pressure. Three riveting pressure strengths of 160, 180, and 200 MPa were set to perform the adhesive riveting tests to analyze the mechanical properties of the three joints. Figures 3a-c show the profiles of the adhesive riveted joints obtained at the three riveting pressures. The head heights were 0.382, 0.212, and 0.153 mm, respectively, indicating that the absolute value of the rivet head height gradually tends to zero as the pressure increases. The internal locking lengths of 0.218, 0.429, and 0.476 mm for the three pressures indicated that as the pressure increases, the rivet

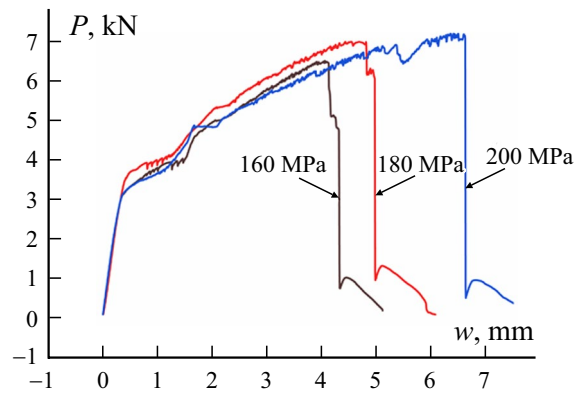


Fig. 4. Load displacement curves $P-w$ at three riveting pressures.

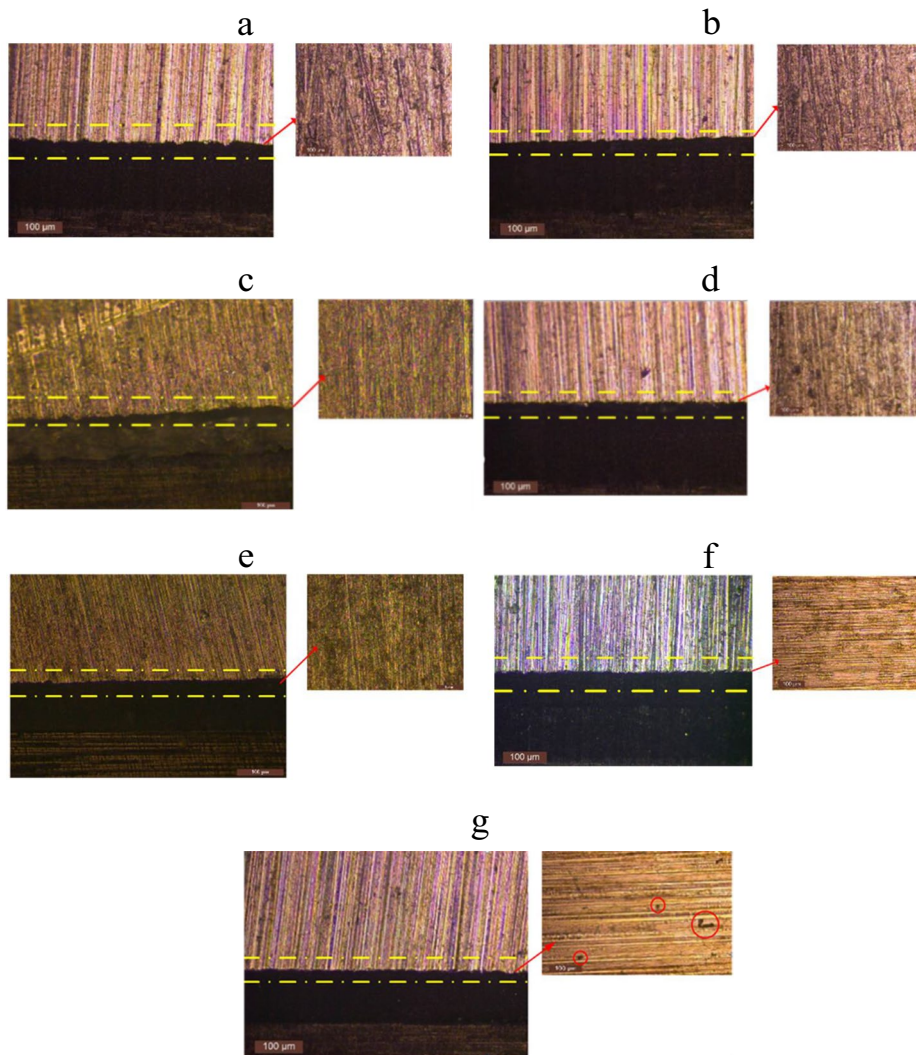


Fig. 5. Profile of riveted-adhesive joints with different surface treatments: 180 (a), 400 (b), 600 (c), 800 (d), 1000 mesh (e), and alcohol (f) and ultrasonic (g) cleaning.

expanded fully and the internal locking length between the rivet and the lower plate increased, which resulted in enhanced interlocking structural properties of the joints, and therefore, the strength of the joint was improved. In addition, the re-

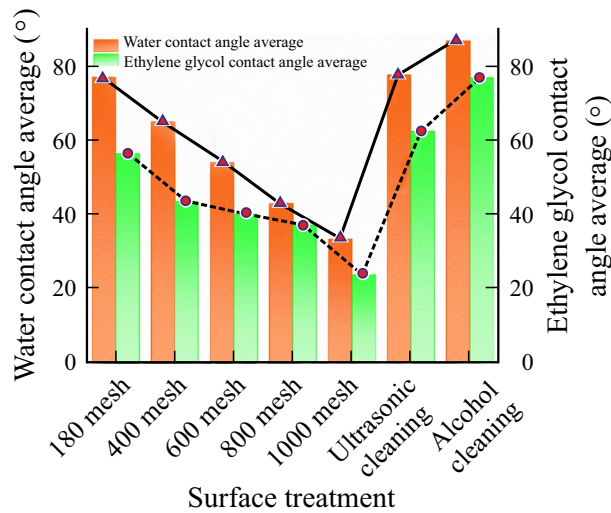


Fig. 6. Average contact angle of water and ethylene glycol.

maining thickness of the adhesive riveting joints under all three pressures was greater than 0.14 mm, which showed that none of the plates had been pierced.

Figure 4 shows the load-displacement curves $P-w$ at the three riveted pressures. In the elastic stage, the slope of the curves of the three riveting pressures was the same, which indicated that the adhesive riveted joints obtained from the three riveting pressures in the tensile initial stage had the same ability to resist elastic deformation. Entering the plastic stage, the adhesive layer gradually failed with the increase of tensile displacement. The maximum tensile shear forces of 6.512, 6.8, and 7.2 kN reached at the three pressures indicate that the ultimate failure load of the joint gradually increased with the increase of riveting pressure. In the end, after the complete failure of the adhesive layer, the rivet carried the main load on the joint failure. The maximum failure load of all three riveting pressure joints reached about 1 kN during the rivet failure stage. In addition, as shown in Fig. 4, the maximum failure displacements of the three riveting pressure joints were 5.113, 6.074, and 7.844 mm, respectively. Thus, the maximum failure displacements were gradually improved with the increase of the pressure. In summary, the change in riveting pressure has a noticeable effect on the mechanical properties of the adhesive riveted joints.

3.1.2. Surface treatment. Figures 5a-e show the shape of the aluminum plate sanded with 180, 400, 600, 800, and 1000 mesh sandpaper respectively, where the yellow boxes are marked as the adhesive sections of the aluminum and CFRP plates. The cross-section of the aluminum plate after sanding showed an undulating profile, and the amplitude of the undulation of the surface profile became smaller with the increase of the sandpaper mesh. The picture indicated by the red arrow on the right was the surface of the aluminum plate; it could be seen that the scratches on the surface after sanding were as crisscrossed as gullies, and the lower the mesh, the more obvious the dents and bumps on the surface of the aluminum plate were. This indicates that the surface area of the aluminum plate also increases, which can enhance the mechanical “interlocking” effect between the surface and the adhesive to a certain extent. Compared with the joint cleaned with alcohol (see Fig. 5g), the joint cleaned with ultrasonic (see Fig. 5f) had some unevenness in the cross-sectional profile of the aluminum plate, and there were deeper pits on the surface of the aluminum plate, which facilitated the formation of mechanical embedding of the adhesive with the surface of the aluminum plate.

The change of free energy of the solid surface has an influence on the solid-liquid contact effect, and the adhesive-plate interface contact belongs to the solid-liquid contact. Therefore, the change of free energy of the plate surface influences the mechanical properties of the adhesive joint. In this paper, the contact angle of AL6061-T6 surface was tested by water and ethylene glycol to obtain the surface energy according to the method of reference [28]. The contact angle is the angle between the tangent line of the gas-liquid interface and the solid-liquid junction line made at the intersection of gas, liquid, and solid phases, and is a measure of the degree of wetting [29]. We used the suspension drop method to measure

TABLE 3. Surface Energy and Roughness under Different Surface Treatments

| Surface treatment | Mesh of sandpaper | | | | | Cleaning | |
|------------------------------------|-------------------|-------|-------|-------|-------|------------|---------|
| | 180 | 400 | 600 | 800 | 1000 | ultrasonic | alcohol |
| Surface energy, mJ/mm ² | 51.17 | 65.97 | 75.85 | 85.13 | 96.15 | 47.62 | 34.67 |
| Roughness, 10 ⁻² μm | 146.3 | 100.3 | 70.63 | 54.63 | 41.17 | 31.40 | 20.20 |

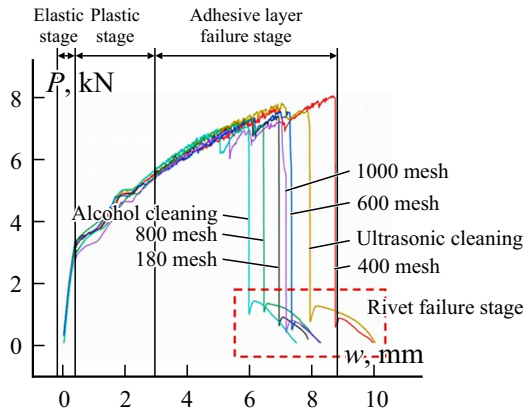


Fig. 7. Load displacement curves $P-w$ for different surface treatments.

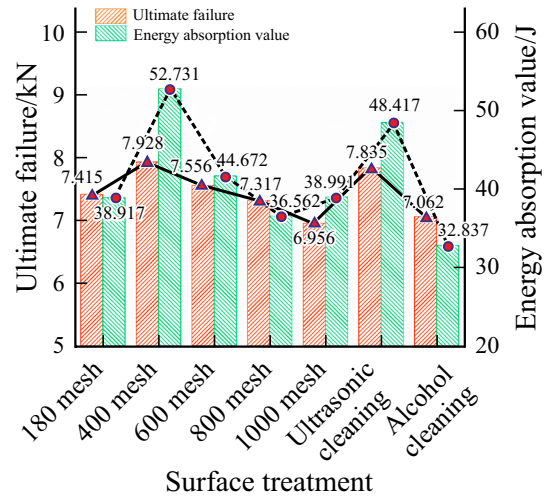


Fig. 8. Mean value of ultimate failure load and energy absorption value.

the contact angles of four different positions on the aluminum plate and took the average value of the contact angles of the four positions as the contact angle of the aluminum plate.

Figure 6 illustrates the average values of contact angles of water and ethylene glycol for aluminum plates with different surface treatments. It could be seen that the contact angle of water and ethylene glycol on the aluminum plate tended to decrease with the increase of sandpaper mesh. This is because the larger the mesh of sandpaper, the finer the sandpaper abrasive, and the relatively shallow and dense scratches on the surface of the aluminum plate, which allows the liquid to better infiltrate the solid surface. The average value of the water contact angle under alcohol cleaning was the largest, 86.3°, while the water and glycol contact angle obtained under ultrasonic cleaning was 77.95 and 62.7°, respectively. This is because ultrasonic cleaning made use of the huge energy released by the cavitation bubble during the collapse to overcome the interaction between the dirt and the oxide film on the surface of the aluminum plate, which could remove the dirt from the surface of the aluminum plate at a deep level, thus allowing the liquid to further infiltrate with the surface.

Table 3 shows the surface energy and roughness obtained from the contact angle calculation. From Table 3, it could be seen that the surface energy and roughness reached the lowest value by using alcohol for cleaning aluminum plate surfaces. For the surfaces treated with sandpaper, the surface energy increased, and the roughness decreased with the increase of the mesh number. The surface performance of aluminum plate cleaned by ultrasonic was also higher than that cleaned by alcohol, but lower than that sanded by sandpaper.

It could be seen from Fig. 7 that the trends of load-displacement curves of joints with different surface treatments in the elastic phase, plastic phase, and the initial phase of adhesive layer failure were approximately the same. However, with the further increase of displacement, the alcohol cleaned adhesive rivet specimen first entered the rivet failure stage, followed by the sandpaper polished specimen, and then the ultrasonically cleaned specimen.

It could be seen in Fig. 8 that the adhesive rivet joints made from alcohol-cleaned aluminum surfaces exhibited lower average values of ultimate failure loads. The strength of the adhesive riveted joints made from aluminum sheets

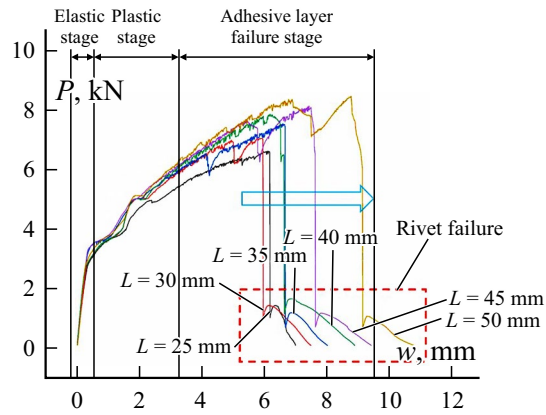


Fig. 9. Load displacement curves for different lap lengths.

sanded with sandpapers ranging from 180 to 1000 mesh showed a trend of first increasing and then gradually decreasing. The strength of joints sanded with 1000 mesh sandpaper was comparable to that treated with alcohol; 400 mesh had the highest performance, and the rest had increased joint strength compared with the alcohol treatment. This was due to the fact that sandpaper sanding increased the surface area of the aluminum plate, increasing the contact area between the aluminum plate and the adhesive.

The strength of the adhesive riveted joints with different sandpaper showed differences. The roughness and surface energy measured and calculated for the surface of the aluminum plate polished with 400 mesh sandpaper were at a medium level, indicating that the interpretation of the strength of the joint should be considered in terms of other aspects. The 180-mesh sandpaper gave the aluminum the largest surface area, but the width and depth of the surface scratches were also relatively large, which helped store air and reduced the actual contact area of the adhesive when bonding to the aluminum, weakening the mechanical “interlocking” effect. The area of aluminum plate obtained by 600, 800, and 1000 mesh was smaller than that obtained by 400 mesh; so, the strength of the joint was reduced. Cleaning the surface of the aluminum plate with ultrasonic could remove the oil spot stains that could not be cleaned off by alcohol wiping, and the continuous ultrasonic waves could destroy the original oxide film on the surface of the aluminum plate, resulting in the ability to properly improve the roughness and surface energy of the aluminum plate. The ultimate failure load and energy absorption values of the adhesive rivet specimens obtained by ultrasonic cleaning were 7.835 kN and 48.417 J, respectively, which were second only to those obtained by 400 mesh sandpaper sanding. In summary, the study shows that suitable sandpaper sanding and ultrasonic cleaning can significantly improve the mechanical properties of the adhesive riveted joints.

3.1.3. Lap length. As shown in Fig. 9, the resistance to deformation of the six groups of specimens was nearly identical in the elastic phase; however, differences began to appear gradually in the plastic phase. During the adhesive layer failure stage, the ultimate failure loads of the six groups of joints fluctuated with increasing displacement, meanwhile, the ultimate failure loads presented an overall upward trend with an increasing lap length, which indicated that changing the lap length had an effect on the strength of the CFRP/aluminum sheet adhesive rivet joint. The arrow noted in Fig. 9 shows that the displacement of the adhesive layer failure increased from 6.18 mm at 25-mm lap length to 9.15 mm at 50-mm lap length, with an improvement of 48%, indicating that as the lap length increased, the displacement of complete failure of the adhesive layer also increased gradually. At the stage of lap failure, there was a large vertical drop in load and then an increase in the process, which was mainly due to the initial cracking of the adhesive of the joint and the bonded plate. And as the displacement increased, the cracks expanded. After the complete failure of the adhesive layer, the load of all six groups of joints dropped sharply to about 1 kN. Then, it was followed by the rivet failure phase, the load would occur a small increase; at this time the rivet played a major role in the strength of the joint. Subsequently, as a result of the destruction of the extruded fiber layer of the rivet, the failure displacement increased by 1~2 mm, and then the load showed a decreasing trend until it reached zero.

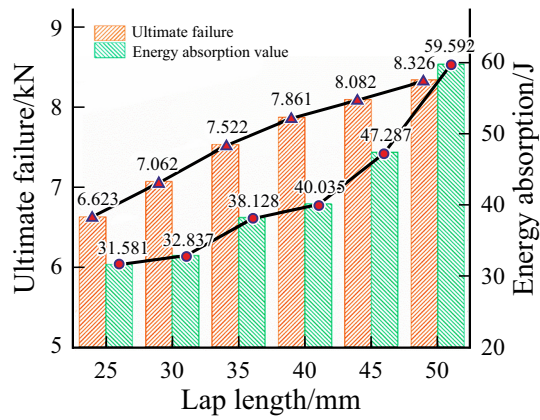


Fig. 10. Mean value of ultimate failure load and energy absorption value.

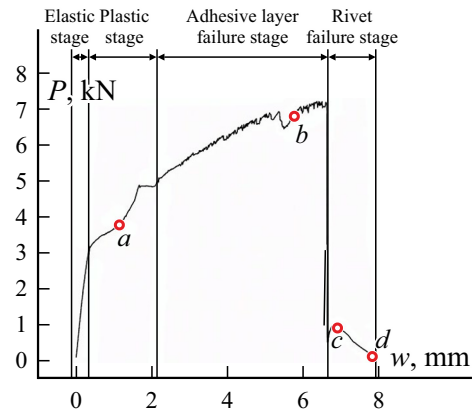


Fig. 11. Load displacement curve $P-w$.

As shown in Fig. 10, the average ultimate failure load of the six specimens increased linearly and gradually from 6.623 kN at 25-mm lap length to 8.326 kN at 50-mm lap length, with an overall increase of 25.71% in peak load. This was due to physical or chemical reactions between the adhesive and the bonding body, which formed mechanical interlocks or created intermolecular forces and chemical bonds, etc., resulting in the upper and lower plates bonding to each other. When the lap length of the joint was increased, these physical and chemical forces were further increased, thus raising the peak ultimate failure load. And as the lap length increased, the energy absorption value of the adhesive riveted joint also increased gradually. For the lap widths between 25 and 40 mm, the energy absorption value increased more slowly, by 26.77%, while for the lap widths between 40 and 50 mm, the energy absorption value increased rapidly by 48.85%. In general, different lap lengths have a significant effect on the mechanical properties of the adhesive riveted joints.

3.2. Failure mechanism of adhesive rivet joints

On the basis of the process parameters, this paper analyzed the failure mechanism of the adhesive riveted joint by selecting a riveting pressure of 200 MPa, a lap length of 30 mm, and the surface of the aluminum plate sanded with 400 mesh sandpaper.

3.2.1. Failure process of joints. Tensile failure process analysis was performed on the adhesive riveted specimens of CFRP-aluminum plates. Figure 11 shows the load-displacement curve of the adhesive riveted joint. The a, b, c, d points on the curve correspond to the four images in Fig. 12. These four points reflect the changes in the tensile-shear process for rivets, CFRP sheets and aluminum sheets. In the elastic and plastic stages, as shown in Fig. 12a, the joint was at the stage of resisting elastic and plastic deformation. The connection between the rivet, the aluminum plate, and the CFRP plate was unchanged. Figure 12b shows the state of the joint during the adhesive layer failure stage. After the initial crack in the adhesive layer developed, the crack continued to expand and subsequently deformation was observed between the rivet leg and the aluminum plate due to extrusion where the separation of the CFRP plate and the end of the aluminum plate occurred. Figure 12c shows the state of the joint at the rivet failure stage, where the aluminum and CFRP plates in the bonding area are completely separated and the rivet side is interlocked with the aluminum plate. Figure 12d shows the overall image of the adhesive rivet joint after complete failure; the rivet is detached from the aluminum plate, and the rivet set on the CFRP plate has a tendency to be detached from the CFRP plate, as marked by the dashed box. The loss of adhesion of the adhesive layer, the failure of the rivet connection structure and the destruction of the material eventually lead to the complete failure of the joint.

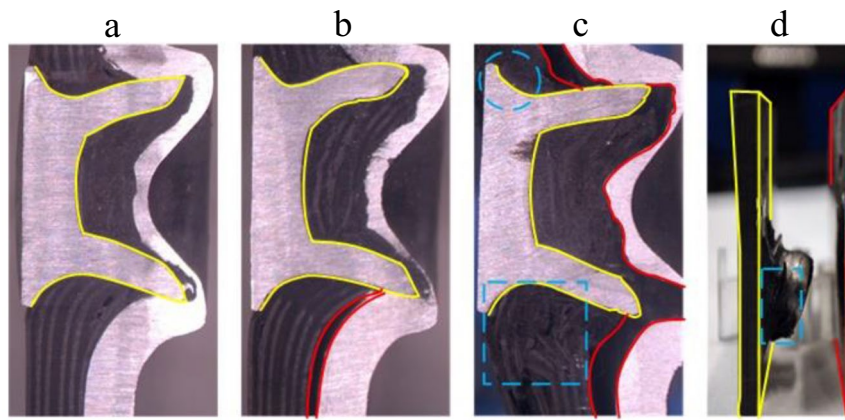


Fig. 12. Failure process of riveted-adhesive joints.

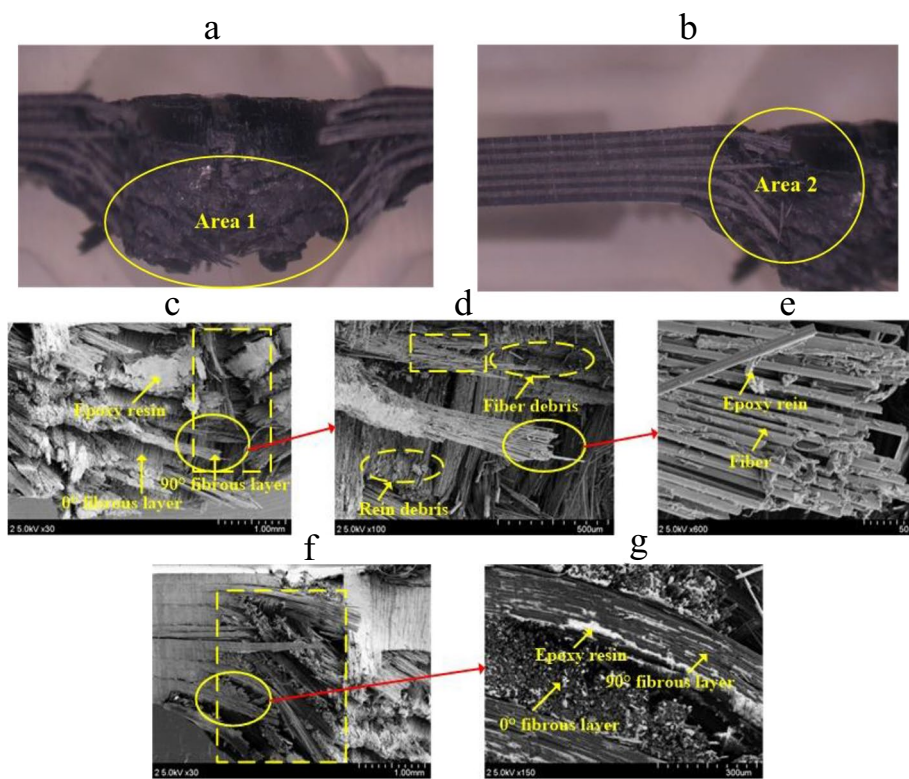


Fig. 13. Morphology of CFRP sheet after failure in Area 1 (a, c, d, e) and Area 2 (b, f, g).

3.2.2. *Failure of CFRP sheet.* The connection of the adhesive riveted joint was mainly through the mechanical interlocking formed by the middle part of the rivet and the upper and lower plates and the adhesive bonding action of the other parts. After the tensile-shear test, the failure mode of the adhesive-riveted specimens of CFRP-aluminum alloy was generally a mixed failure mode in which the aluminum plate was detached from the CFRP plate and rivet, while the adhesive layer is for interfacial damage and cohesive damage. After the failure of the joint, a large amount of adhesive remained on the surface of the CFRP plate.

Figures 13c-e show the microscopic view of Area 1 in Fig. 13a. The matrix and reinforcement of the CFRP sheet around the rivet in Fig. 13a had collapsed severely, and the layers with fibers oriented at 0° and 90° were relaxed under the tensile force and rivet pressure, thus making the delamination severe. The 90° -fiber bundle was pulled off as observed in

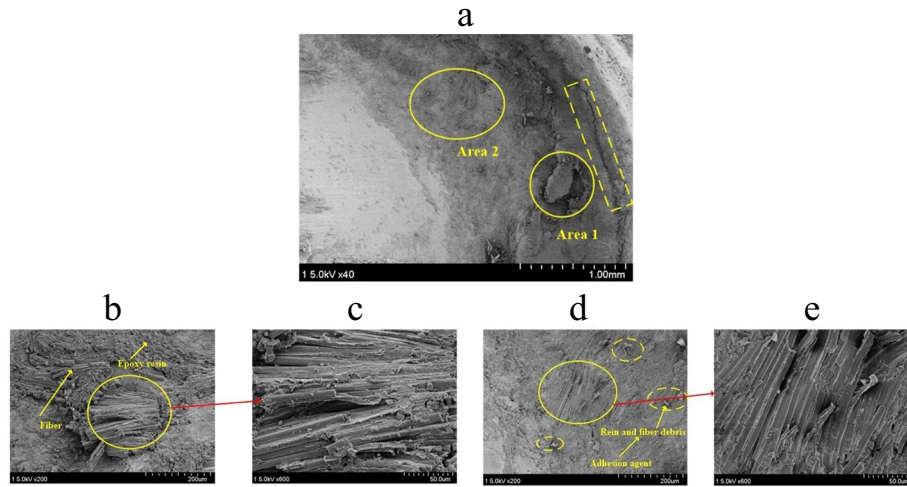


Fig. 14. Morphology of aluminum sheet after failure in Area 1 (a, b, c) and Area 2 (a, d, e).

the dashed box in Fig. 13c, resulting in the enlargement of the rivet hole formed in the CFRP sheet. The presence of resin and fiber debris in the circular dashed box from Fig. 13d was found to be caused by the puncture of the CFRP sheet during the riveting test and by extrusion during the tensile-shear test. The fibers in Fig. 13e were separated from each other between the fiber bundles, and there was no longer any adhesion between the resin and the fibers. Figures 13f and 13g show the microscopic view of Area 2 in Fig. 13b. The delamination and damage of the CFRP sheet after joint stretching could be clearly observed in Fig. 13f, and the closer to the lower surface of the CFRP sheet the more severe the delamination and damage was. Subsequently, the CFRP plate after failure was further magnified and observed, and it was found that the CFRP plate around the rivet was severely damaged in the tensile-shear test, and the rivet hole became larger, making the joint load-bearing capacity decrease until it disappeared.

3.2.3. Failure of aluminum sheet. For the adhesive riveted joint after failure, the surface of the undeformed aluminum plate remained adhesive and matrix, while the middle part of the aluminum plate has changed dramatically in form. The cracking of the aluminum plate observed in Fig. 14a is due to the continued pressure on the aluminum plate after the rivet pierced the upper plate, which caused the flow and deformation of the material in the concave die. In addition, the aluminum plate in contact with the rivet legs during stretching was subjected to pressure from the rivet legs, which also led to the creation of cracks.

Figures 14b and 14c show the magnified microscopic images of Area 1. Due to the adhesive between the CFRP plate and the aluminum plate, a large number of fibers and epoxy resin in a block-like random distribution could be observed on the surface of the aluminum plate. The block-shaped composite was magnified 600 times for observation. Here, the fibers and resin were still better bonded together due to the fact that the CFRP sheet was broken by the rivet leg tip during the riveting stage and moved with the rivet to the upper surface of the aluminum sheet, where it was finally bonded to the aluminum sheet by the adhesive. Figures 14d and 14e show the magnified microscopic view of Area 2, where less composite material remained. From the circular dashed line marking, it could be observed that fiber and resin debris were scattered on the surface of the aluminum plate. In addition, it could be found that most of the composite material at the rivet hollow was separated from the aluminum plate, leaving groove-like adhesive on the surface of the aluminum plate, as shown in Fig. 14e.

The joint in the riveting process due to the large riveting pressure made a large part of the adhesive at the rivet is extruded to the area around the rivet. In addition, due to the poor mobility of the composite material, the adhesive between the CFRP plate and the aluminum plate at the hollow part of the rivet leg failed to form a good adhesive interface with the upper and lower plates. Therefore, when the other parts of the adhesive layer completely failed, only the rivet in the middle part played a major role in bearing the strength of the joint.

4. Conclusions

CFRP plate and 6061-T6 aluminum alloy were used as research objects to explore the mechanical properties and failure mechanisms of self-piercing riveted-bonded joints of composite and aluminum alloys. The main results of the investigation can be summarized as follows.

(1) Adhesive riveted specimens with different riveting pressures had the same ability to resist elastic deformation in the elastic phase. However, as the riveting pressure increased, the ultimate failure load and failure displacement of the joint also increased.

(2) The surface of the aluminum plate using sandpapers with different mesh numbers for grinding or ultrasonic cleaning helped the adhesive and interface to form a mechanical “interlocking” effect, which helped the surface area, roughness, and surface energy of the aluminum plate to be improved in varying degrees, thus making the mechanical properties of the joint higher than the mechanical properties of the joint after alcohol cleaning.

(3) Increasing the lap length could improve the ultimate failure load and failure displacement of the adhesive riveted specimen, and its energy absorption value was also improved. However, when the increased value exceeds a certain range, the range of the rubber layer in the middle region not subjected to external load became larger, and at this time, increasing the lap length was not very meaningful to improve the strength of the joint.

(4) The adhesive rivet specimen failure process was from adhesive layer failure to rivet failure. After the failure of the adhesive layer, the CFRP plate collapsed and delaminated severely, and could not bear the external load. The surface of the aluminum plate with large deformation also shows cracks and a large number of fibers and resin, which failed to produce good adhesion with the composite material, and the middle part was mainly carried by rivets at this time. When the rivet failed, the joint failed completely.

Acknowledgement. This work was supported by the Natural Science Foundation of Shanghai (Grant No. 20ZR1422600) and Shanghai Technical Innovation Project Foundation (Grant No. 21DZ2204300).

REFERENCES

1. D. M. Baskin, “The automotive body lightweighting design philosophy,” *Lightweight Compos. Struct. in Transport*, 75-90 (2016).
2. H. Zhang, L. Zhang, Z. Liu, and P. Zhu, “Research in failure behaviors of hybrid single lap aluminum-CFRP (plain woven) joints,” *Thin-Walled Struct.*, **161** (2021).
3. M. Li, T. Su, Y. Chen, H. He, and X. Yang, “Salt spray aging effects on dynamic responses and failure characteristics of hybrid bonded-riveted CFRP/Al joints under high speed loading,” *J. Manufact. Processes*, **72**, 582-593 (2021).
4. A. Pramanik, A. K. Basak, Y. Dong, P. K. Sarker, M. S. Uddin, G. Littlefair, A. R. Dixit, and S. Chattopadhyaya, “Joining of carbon fibre reinforced polymer (CFRP) composites and aluminium alloys – A review,” *Compos., Part A*, **101**, 1-29 (2017).
5. H. Xia, Y. Ma, C. Chen, J. Su, C. Zhang, C. Tan, L. Li, P. Geng, and N. Ma, “Influence of laser welding power on steel/CFRP lap joint fracture behaviors,” *Compos. Struct.*, **285** (2022).
6. A. Rudawska, “Adhesive joint strength of hybrid assemblies: Titanium sheet-composites and aluminum sheet-composites—Experimental and numerical verification,” *Int. J. Adhesion and Adhesives.*, **30**, No. 7, 574-582 (2010).
7. R. A. Pethrick, “Design and ageing of adhesives for structural adhesive bonding – A review,” *Proc. Institution of Mech. Engineers, Part L: J. Mater.: Design and Applications.*, **229**, No. 5, 349-379 (2014).
8. J. D. Jimenez-Vicaria, M. D. Pulido, and D. Castro-Fresno, “Influence of carbon fiber stiffness and adhesive ductility on CFRP-steel adhesive joints with short bond lengths,” *Construction and Building Mater.*, **260** (2020).
9. Y. Cao, Z. Cao, Y. Zuo, L. Huo, J. Qiu, and D. Zuo, “Numerical and experimental investigation of fitting tolerance effects on damage and failure of CFRP/Ti double-lap single-bolt joints,” *Aerospace Sci. and Technol.*, **78**, 461-470 (2018).

10. S. Li, S. Zhang, H. Li, X. Qin, X. Wu, and L. Gui, "Numerical and experimental investigation of fitting tolerance effects on bearing strength of CFRP/Al single-lap blind riveted joints," *Compos. Struct.*, **281** (2022).
11. G. Zhang, Q. Zhu, H. Yang, C. Yang, Y. Liu, and C. Wang, "Effect of surface treatments on the laser welding performance of dissimilar materials," *J. Manufact. Processes.*, **74**, 465-473 (2022).
12. M. A. Karim, J. H. Bae, D. H. Kam, C. Kim, W. H. Choi, and Y. D. Park, "Assessment of rivet coating corrosion effect on strength degradation of CFRP/aluminum self-piercing riveted joints," *Surface & Coatings Technol.*, **393** (2020).
13. M. Li, W. Luo, Y. Chen, and X. Yang, "Full-field strain distribution and failure characteristics of CFRP-repaired steel structures," *Eng. Failure Analysis.*, **115** (2020).
14. G. D. Franco, L. Fratini, and A. Pasta, "Influence of Parameters in a Hybrid Joints (SPR/Bonded) GFRP-Aluminum," *Key Eng. Mater.*, **554-557**, 1031-1036 (2013).
15. N. Chowdhury, W. K. Chiu, J. Wang, and P. Chang, "Static and fatigue testing thin riveted, bonded and hybrid carbon fiber double lap joints used in aircraft structures," *Compos. Struct.*, **121**, 315-323 (2015).
16. P. Lopez-Cruz, J. Laliberté, and L. Lessard, "Investigation of bolted/bonded composite joint behaviour using design of experiments," *Compos. Struct.*, **170**, 192-201 (2017).
17. Y. Chen, X. Yang, M. Li, K. Wei, and S. Li, "Mechanical behavior and progressive failure analysis of riveted, bonded and hybrid joints with CFRP-aluminum dissimilar materials," *Thin Walled Struct.*, **139**, 271-280 (2019).
18. P. V. Inbanaathan, B. Dhinesh, U. Tamilarasan, B. R. Venkatesh Prasanna, C. Dineshkumar, and S. Kiran, "Characteristics assessment on riveted, bonded and hybrid joints using GFRP composites," *Mater. Today: Proceedings*, **47**, No. 19, 6889-6895 (2021).
19. G. D. Franco, L. Fratini, and A. Pasta, "Analysis of the mechanical performance of hybrid (SPR/bonded) single-lap joints between CFRP panels and aluminum blanks," *Int. J. Adhesion and Adhesives.*, **41**, 24-32 (2013).
20. G. Marannano and B. Zuccarello, "Numerical experimental analysis of hybrid double lap aluminum-CFRP joints," *Compos., Part B*, **71**, 28-39 (2015).
21. Y. Liu and W. Zhuang, "Self-piercing riveted-bonded hybrid joining of carbon fibre reinforced polymers and aluminium alloy sheets," *Thin-Walled Struct.*, **144** (2019).
22. G. D. Franco, L. Fratini and A. Pasta, "Fatigue strength of a single lap joint SPR-bonded," *American Institute of Physics*, **1353**, 1265-1271 (2011).
23. G. D. Franco, L. Fratini, and A. Pasta, "Influence of the distance between rivets in self-piercing riveting bonded joints made of carbon fiber panels and AA2024 blanks," *Mater. and Design.*, **35**, 342-349 (2012).
24. V. Fiore, F. Alagna, G. Galtieri, C. Borsellino, G. D. Bella, and A. Valenza, "Effect of curing time on the performances of hybrid/mixed joints," *Compos., Part B*, **45**, No. 1, 911-918 (2013).
25. M. Rośkiewicz, J. Godzimirski, A. Komorek, J. Gąsior, and M. Jaształ, "Influence of the arrangement of mechanical fasteners on the static strength and fatigue life of hybrid joints," *Mater.*, **13**, No. 23, 5308 (2020).
26. J. Cui, S. Gao, H. Jiang, X. Huang, G. Lu, and G. Li, "Adhesive bond-electromagnetic rivet hybrid joining technique for CFRP/Al structure: Process, design and property," *Compos. Struct.*, **244** (2020).
27. Y. Lu, "Study on the process and mechanical properties of glued and riveted joints of aluminum and steel sheet," [in Chinese], Shanghai University of Eng. Sci., 2020.
28. X. P. Wang, Y. Z. Liao, H. H. Guan, C. L. Gao, M. H. Zhu, X. Y. Jin, C. Xu, J. H. Du, and W. B. Xue, Study on the oxidation behavior of high-temperature steam in micro-arc oxide film at 1000~1200°C on zirconium surface [in Chinese], *Surface Technology*, Chong Qing (2021).
29. T. Y. Zhao and L. Jiang, "Contact angle measurement of natural materials," *Colloids and Surface B: Biointerfaces*, **161**, 324-330(2018).